Translational dynamics of water in a nanoporous layered silicate

Sankar Nair*
School of Chemical & Biomolecular Engineering, Georgia Institute of Technology, Atlanta, Georgia 30332-0100, USA

Zema Chowdhuri, Inmaculada Peral, and Dan A. Neumann
NIST Center for Neutron Research, National Institute of Standards & Technology, Gaithersburg, Maryland 20899-8562, USA

L. Charles Dickinson
Department of Polymer Science & Engineering, University of Massachusetts, Amherst, Massachusetts 01003-4530, USA

Geoffrey Tompsett
Department of Chemical Engineering, University of Massachusetts, Amherst, Massachusetts 01003-9303, USA

Hae-Kwon Jeong and Michael Tsapatsis
Department of Chemical Engineering & Materials Science, University of Minnesota, Minneapolis, Minnesota 55455-0132, USA
(Received 20 July 2004; revised manuscript received 15 November 2004; published 23 March 2005)

Neutron time-of-flight and backscattering spectroscopy have been used to study the translational diffusion of water molecules in the unusual layered material AMH-3, which consists of (zeolitelike) three-dimensionally nanoporous silicate layers spaced by (claylike) interlayer regions. The synthesis of AMH-3 and its characterization by ^{29}Si NMR, Raman, and infrared spectroscopy, are described. An analysis of quasielastic neutron scattering (QENS) spectra using the random jump diffusion model reveals two translational diffusive motions clearly separated in time scales: a fast process ($D \sim 10^{-9}$ m^2/s at 300 K), and a much slower process ($D \sim 10^{-11}$ m^2/s at 300 K). Considering the structural model of AMH-3 and the transport properties extracted from the QENS data, it is suggested that the slower motion corresponds to diffusion by water molecules in the interlayer spaces whereas the fast process involves diffusion in the silicate layer. This first investigation of transport phenomena in nanoporous layered silicates like AMH-3 indicates that they have the potential to offer mass transport properties different from zeolite materials and layered clays.

DOI: 10.1103/PhysRevB.71.104301 PACS number(s): 61.12.Ex, 82.56.Ub, 82.75.Jn, 82.80.Gk

I. INTRODUCTION

Crystalline nanoporous materials like the aluminosilicate zeolites are of technological importance as molecular sieves, nanostructured host materials, and selective catalysts.[1] As a result, there are a number of investigations[2–4] of the structural and transport properties of guest-host systems consisting of molecules such as water, permanent gases, hydrocarbons, and other industrially significant molecules confined in nanoporous framework materials. Layered materials composed of nonporous oxide layers spaced by hydrated ions, are also currently of interest as model systems to investigate the diffusion of molecules, particularly water, in confined environments.[5–8] They have also found applications in the development of nanocomposite materials with enhanced mechanical and thermal stability. On the other hand, a small but growing number of nanoporous layered materials[9–12] show potential for new technological applications. Like nonporous layered clays, they are composed of oxide (e.g., silicate or aluminophosphate) layers spaced by metallic or organic cations. However, the individual layers contain pore spaces similar to zeolites and other nanoporous frameworks. An important potential application of these novel materials is based on exfoliating the layers and processing them with polymers, to produce thin nanocomposite membranes[9,13] that combine the molecular sieving properties of the nanoscopic layers with the processability and mechanical strength of the polymer. Additionally, nanoporous layered materials are interesting model systems in that they provide two well-defined, and possibly interacting, environments for confined transport of molecules.

An example of a nanoporous layered material is the recently reported layered silicate AMH-3 (Fig. 1).[9] It contains porous silicate layers with eight-membered rings in all three principal crystal directions. The as-synthesized material has the unit cell formula $Na_8Sr_8Si_{32}O_{76} \cdot 16H_2O$ and contains about 9% water by mass (16 water molecules per unit cell). The water molecules are distributed in equal numbers over two adsorption sites (*S*1 and *S*2) located near the sodium (Na^+) and strontium (Sr^{+2}) cations. The site *S*1 is located in the interlayer space, whereas *S*2 is located within the porous layer. The nearest neighbor *S*1-*S*1, *S*2-*S*2, and *S*1-*S*2 crystallographic distances are 4.3, 3.8, and 3.5 Å, respectively. Water can diffuse within the interlayer spaces and within the porous layers. A transport path between interlayer regions is also available through the layer, *via* diffusive jumps between *S*1 and *S*2 sites. Thus, it is expected that diffusion in AMH-3 would show significantly different characteristics in comparison to porous framework materials like zeolites and layered clay materials. In this paper we present an experimental investigation of jump diffusion processes in this technologically important class of new materials, using the AMH-3/water complex as the model system.

 ©2005 The American Physical Society

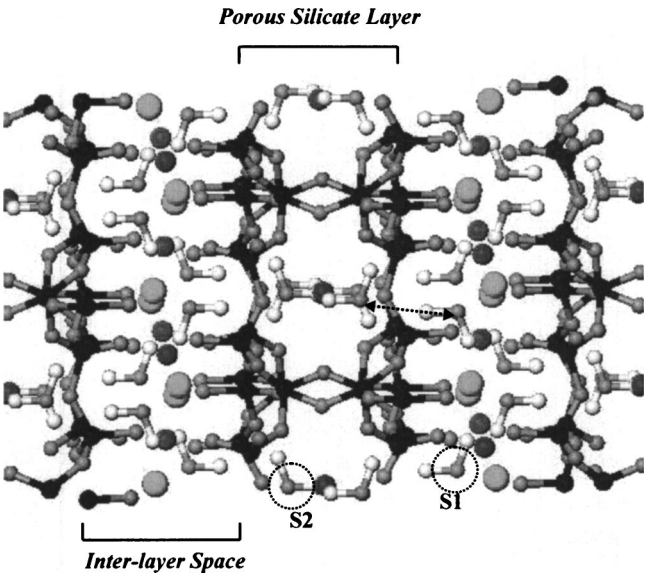

FIG. 1. Structure of AMH-3 viewed down [001], showing the porous silicate layers and the interlayer spaces. Water molecules are on adsorption sites *S*1 (bound to Na^+ and Sr^{+2} in the interlayer) and *S*2 (bound to Na^+ in the layer). There are eight water molecules per unit cell (of volume 2.145 nm^3) in each type of site. Jumps between *S*1 sites can occur in the interlayer spaces, and between *S*2 sites in the porous layers. An *S*1-*S*2 jump is also possible through an eight-membered ring of the porous layer (dashed arrow). Crystallographic nearest-neighbor jump distances are given in the text.

The paper is organized as follows. In Sec. II we describe the experimental details of AMH-3 synthesis and characterization. In Sec. III, we present a brief discussion of the synthesis of AMH-3 including an exploration of the synthesis parameter space. In Sec. IV, we characterize the material by an assignment of its ^{29}Si NMR, Raman and infrared spectra. The water transport properties of AMH-3 are then studied in Sec. V by a combination of neutron time-of-flight and backscattering spectroscopy to probe water diffusion processes over a ~1–500 ps time scale. It is shown that in contrast to clays and zeolite materials, there are two translational jump processes observable by quasielastic neutron scattering, on the nanosecond and picosecond time scales, respectively. We summarize our conclusions in Sec. VI.

II. EXPERIMENTAL DETAILS

AMH-3 was obtained as a crystalline powder using the synthesis and purification methods described recently[9] (see also Sec. III). Raman spectra were obtained using a Bruker FT-Raman equipped with an Nd-YAG (1064 nm), an incident power of 100 W, and averaging of 400 scans to a single spectrum. FT-IR spectroscopy was undertaken with a Bruker Equinox 5 spectrometer, using a resolution of 4 cm^{-1} and averaging of 50 scans to a single spectrum. Samples were prepared as KBr pellets of 12.5 mm diameter using approximately 1 wt % sample. The ^{29}Si CP/MAS NMR spectrum was collected on a Bruker DSX300 spectrometer with a MAS probe at room temperature. The 29Si CP/MAS NMR spectrum was collected on a Bruker DX300 Spectrometer with a MAS probe at room temperature. Cross-polarization (CP) was performed with 41.7 kHz Hartmann-Hahn matching for 2 ms, and a 6 μs proton pulse, spinning at 2500 Hz. The chemical shift anisotropy of each site was determined by spinning at 900 Hz and fitting the sideband intensity pattern utilizing the MAS fitting tool of Bruker XWINNMR software.

For neutron scattering measurements, the sample was distributed as a ~1 mm thin layer over one half of an aluminum foil. The other half was folded over the sample and closed at the edges to produce a waferlike sample. This formed the inner lining of a cylindrical aluminum sample can, which was sealed under helium with a lead O-ring. A closed cycle refrigerator maintained the temperature to a precision of ± 1 K. Time-of-flight measurements were performed on the disk chopper time-of-flight spectrometer[14] (DCS) at NIST, operating at an incident neutron wavelength of 9 Å, giving a resolution ~22 μeV in terms of the full width half maximum (FWHM). Backscattering spectra were measured on the high-flux backscattering spectrometer[15] (HFBS) at NIST, with an energy transfer window of ±36 μeV and a resolution of ~1 μeV. Data reduction and analysis was performed with the DAVE[16] package. The spectra were normalized to the beam monitor and a detector efficiency correction was applied using a vanadium standard. In the case of the time-of-flight data, detectors showing strong diffraction from the crystal structure were masked during reduction. Resolution functions of both spectrometers were measured using a vanadium standard, and were each well fitted by two Gaussians.

III. SYNTHESIS OF AMH-3

To ascertain the region of compositional space in which AMH-3 can be obtained, and to explore the possibility of obtaining new structural materials related to AMH-3, we have varied the synthesis parameters systematically. The synthesis was carried out using the previously reported procedure.[9] The molar composition of the synthesis solution was x TiO_2: 10 SiO_2: y $SrCl_2$: z NaOH: 675 H_2O, where x, y, and z were varied to generate 15 different compositions. Powder x-ray diffraction patterns were taken for preliminary characterization of the phases obtained. Figure 2 summarizes the synthesis parametric investigation. We find that the presence of a titanium species is critical for the formation of AMH-3, although the material itself contains no titanium. Additionally, there are windows in the parameter maps where one can synthesize crystalline AMH-3 along with an amorphous phase which can later be separated to give pure AMH-3. Certain combinations of the parameters led to the formation of other crystalline phases. One of these phases, AMH-2, is a new open framework titanosilicate whose structure has been solved by single-crystal x-ray diffraction and will be reported elsewhere. Another unknown crystalline phase has been obtained, but its structure has not been solved so far due to the absence of sufficiently large single crystals and the presence of impurity phases that complicate its structure solution by powder methods. A further investigation is currently underway to explore the parameter domains which

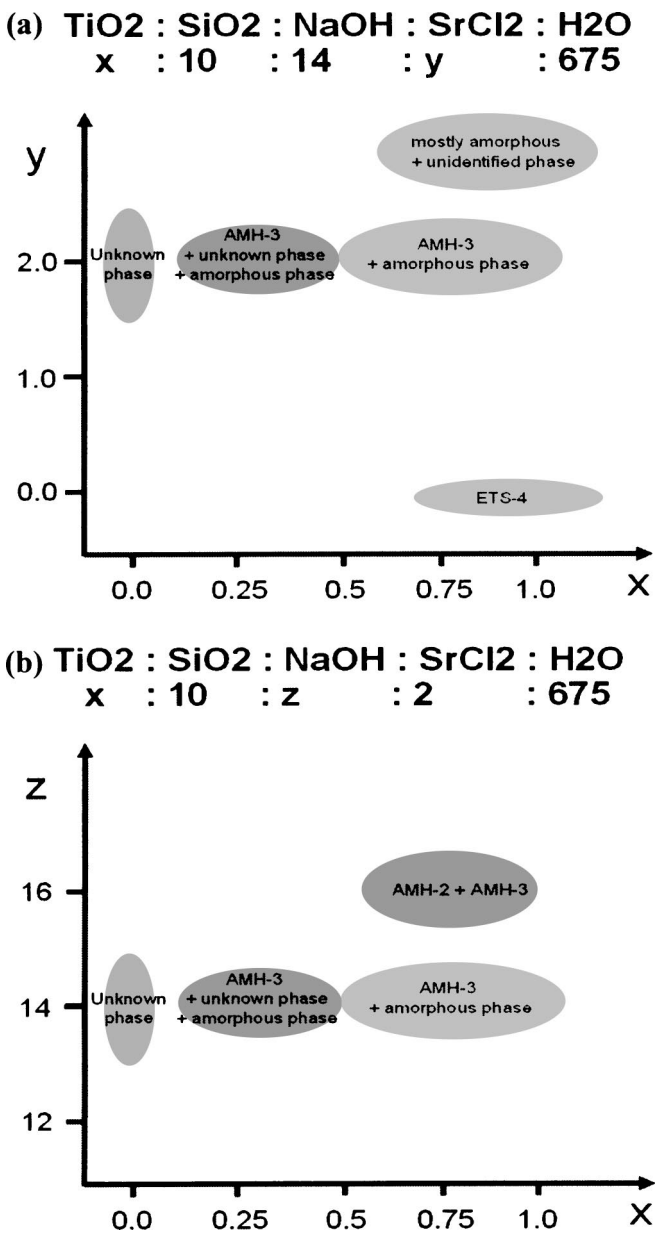

FIG. 2. Synthesis parameter maps with respect to (a) relative amounts of titanium and strontium, and (b) relative amount of titanium and sodium. AMH-2 is an open framework titanosilicate.

may lead us to discover new layered materials and framework materials.

IV. NMR AND VIBRATIONAL SPECTRA OF AMH-3

Valuable information about the local structure can be obtained by solid state CP/MAS NMR spectroscopy. We previously solved the structure of AMH-3 by powder x-ray diffraction methods and reported preliminary ^{29}Si NMR spectra that were consistent with the structural model. There are three resonances at −89.4, −90.8, and −93.5 ppm (Fig. 3) with an intensity ratio of 2.11:1.28:1.00. We have previously assigned the two lowest chemical shifts to the three Q3 silicons and the highest to the Q4 silicon.[9] In this study, we have

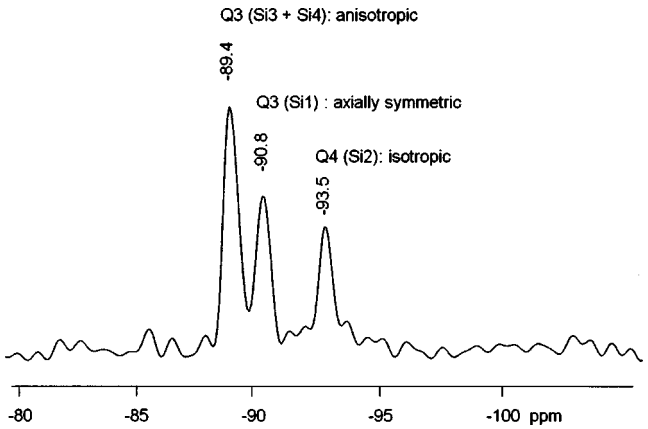

FIG. 3. ^{29}Si solid state CP/MAS NMR spectrum of AMH-3.

fitted the chemical shift anisotropies of the ^{29}Si nuclear sites to verify our previous assignments. Depending on the local site symmetry, the chemical shift may be anisotropic with respect to the orientation of the crystals in the applied magnetic field.[17] Therefore, the chemical shift anisotropy gives valuable information regarding the local symmetry of the nuclear sites. We found that the −93.5 ppm resonance is totally isotropic, which corroborates the tetrahedral site symmetry of the Q4 silicon (Si2). The next resonance at −90.8 ppm is axially symmetric with principal values of −64.76 and −141.02 ppm. We have assigned this resonance to the Q3 site Si1. This is due to the pseudo-mirror plane dissecting Si2 and Si1 sites, resulting in the Si3 and Si4 sites on each side. This local symmetry at the Si1 site leads to the axially symmetric chemical shift anisotropy. The third and most intense resonance at −89.4 ppm is anisotropic with principal values of −58.04, −74.34, and −136.89 ppm. We assigned this resonance to the two remaining Q3 silicons Si3 and Si4, which are topologically identical within the 4MR building unit of AMH-3. The anisotropy of Si3 and Si4 is not surprising, considering that there is no local symmetry associated with these nuclear sites.

Figures 4(a) and 4(b) show the IR and Raman spectra of AMH-3. Vibrational spectra in the region of 200 to 1300 cm^{-1} are important tools to verify the structural features of nanoporous framework oxides like zeolites, which are typically determined by x-ray crystallography.[18,19] Zeolites are built of interconnected $[TO_4]$ tetrahedra (e.g., T = Si or Al). The original IR band assignments[18] make a distinction between external and internal vibrations of the TO_4 tetrahedra. The vibrations due to the external linkages are often very sensitive to the structural details. The band assignments of the main IR bands for zeolite frameworks are summarized in Table I. Akin to zeolites, AMH-3 is built of interconnected $[SiO_4]$ tetrahedra within layers, and these layers are held together by the strontium and sodium cations between them.[9] It is therefore expected that rather similar assignments of vibration bands can be made. The assigned bands of the Raman and IR spectra of AMH-3 are listed in Table II, which also summarizes the structural information and factor group analysis. Despite the absence of zeolitelike double rings (e.g., D4R and D6R) in the AMH-3 structure, there are bands between 650 and 500 cm^{-1}. We have tenta-

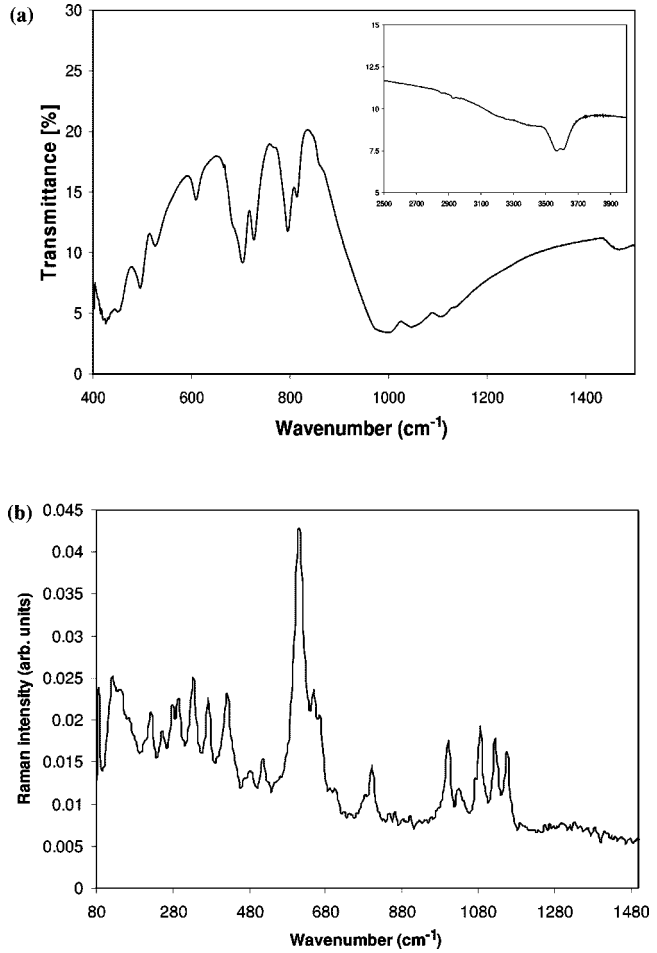

FIG. 4. (a) FTIR spectrum of AMH-3. (b) FT-Raman spectrum of AMH-3.

tively assigned these bands as due to the single four-membered rings (S4R) within the layers. Since typical vibrations of cations in the zeolites are in the far-IR region (200–50 cm^{-1}), we have assigned Na-O stretching modes to the bands below 300 cm^{-1} (Refs. 18–20). The bands between 400 and 300 cm^{-1} were assigned to Sr-O stretching modes in the [SrO6] octahedra and pore opening modes of the eight-membered rings (S8R).[18,20] The inset of Fig. 4(a) shows the near-IR region of the spectrum. There are two distinct hydroxyl stretching modes of equal intensity at 3561 and 3645 cm^{-1}, respectively, suggesting the existence of two sites (*S*1 and *S*2) for bound water. The complete absence of a terminal SiO-H (silanol) stretching band which occurs in zeolites at ~3720 cm^{-1} is consistent with the structure of AMH-3 previously determined by powder x-ray diffraction.[9,20] According to this structure, the terminal oxygen anions of the porous layers are balanced by the strontium and sodium cations in the structure, so that a significant number of hydroxyl groups do not exist in the material.

V. WATER DIFFUSION IN AMH-3

The quasielastic neutron scattering model used in this study is the random jump diffusion (RJD) model, which has been found to describe the dynamics of water in pure form as well as confined in mesoporous glasses, zeolites, aqueous polymer solutions, clays, and on protein surfaces.[21–26] In the RJD model, a molecule resides at an adsorption site for a time τ_0 followed by a jump to a neighboring site, with a random distribution of jump distances. During time τ_0, the molecules also undergo vibrations and rotations around the adsorption site. If the rotational and translational motions are assumed to be uncoupled, the intermediate scattering function is $I(Q,t)=W(Q)F^R(Q)F^T(Q)$.[21–26] The first term is the isotropic Debye-Waller factor $W(Q)=\exp[-U^2Q^2/3]$. Rotational motions can be described approximately by $F^R(Q,t)=j_0^2(Qb)+3j_1^2(Qb)e^{-t/3\tau_{ROT}}+\cdots$, where b is the O-H bond length (~1 Å) and τ_{ROT} is the relaxation time for reorientations.[27] The translational part of the intermediate scattering function in the RJD model is $F^T(Q)=\exp[-\Gamma(Q)t]$, with $\Gamma(Q)=DQ^2/(1+DQ^2\tau_0)$ being the half-width half maximum (HWHM) of the quasi-elastic part of the spectrum. The diffusivity (D) associated with this jump is related to the mean-square jump length $l^2\approx 6D\tau_0$. Transforming $I(Q,t)$ to the energy-transfer domain, the dynamic structure factor $S(Q,E)=W(Q)[j_0^2(Qb)L(\Gamma(Q))+3j_1^2(Qb)L(\Gamma(Q)+1/3\tau_{ROT})+\cdots]$ is obtained, where E is the energy transfer. Considering only the first two terms of this expansion, the structure factor is found to be a sum of two Lorentzian functions. The first has a Q-dependent half-width $\Gamma(Q)$ arising from translational motion, while the second has a half-width of $\Gamma(Q)+1/3\tau_{ROT}$, due to both translational and rotational motions. If the Q-range is chosen to be low ($\leqslant$1.0 Å^{-1}), j_1 and higher order terms are small in comparison to the time-independent term.[22,28] Thus the experimental conditions can be chosen to minimize the rotational contribution to the quasielastic scattering and probe the translational dynamics, which is of primary interest here.

TABLE I. Band assignments in framework oxide materials.

Internal tetrahedra		External linkages	
Band (cm^{-1})	Assignment	Band (cm^{-1})	Assignments
1250–950	Asymmetrical stretch	650–500	Double ring
720–650	Symmetrical stretch	300–420	Pore opening
420–500	T-O bend	750–820	Symmetrical stretch
		1050–1150	Asymmetrical stretch

TABLE II. Assignment of vibrational spectra of AMH-3 [space group $C2/c$ (No. 15); 174 total atoms in the Bravais cell; 171 predicted vibrational modes; 87 Raman modes ($43A_g+44B_g$) and 84 IR modes ($42A_u+43B_u$); no inactive or coincident modes].

FT-IR	FT-Raman	Assignments
	120	δ(Si-O-Si) bending mode and ν(Na-O)
	152	"
	162	"
	202	"
	222	"
	251	"
	278	"
	293	ν(Sr-O) or pore opening (S8R)
	332	"
	370	"
421	420	δ(Si-O) bending mode
449	444	"
	469	ν_s(Si-O-Si) in S4R
494	482	"
525	513	"
600	609	ν_s(Si-O) symmetric stretch (S4R)
	648	ν_s(Si-O) symmetric stretch
680	661	"
702	702	"
725	781	"
793	800	ν_s(Si-O) symmetric stretching (external linkage)
820		"
882		"
995	999	ν_{as}(Si-O) asymmetric stretching
1049	1026	"
1018	1072	"
	1084	"
	1122	"
	1155	"
1649		H-O-H scissoring mode, adsorbed water
3561		O-H stretch, adsorbed water
3645		O-H stretch, adsorbed water

Figure 5(a) shows an example of time-of-flight spectra taken on DCS at 300 K. To reliably probe any fast translational motions on the picosecond time scale, we use an incident neutron wavelength of 9 Å (for a high energy resolution and a reasonably high neutron flux). Since we are primarily interested in the translational dynamics, the data analysis is confined to seven spectra with $Q \leqslant 1.05$ Å^{-1} so that rotational contributions can be neglected. A resolution-broadened delta function models coherent scattering contributions. A linear background is also included. The quasielastic component is initially fitted with a single Lorentzian function, which gave an excellent fit to the data. To verify that the rotational contribution is negligible, the full two-Lorentzian

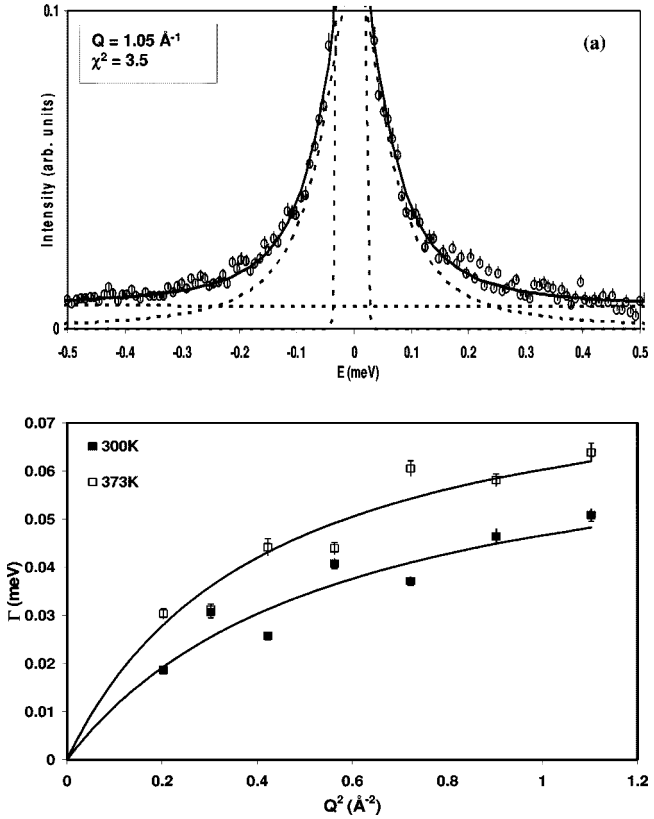

FIG. 5. (a) An example of the QENS spectrum from DCS showing measured data and fitted components. (b) HWHM of quasielastic spectral component measured on DCS at two temperatures. The fits to the RJD model are also shown as solid lines (after convolution with the instrumental resolution function).

model mentioned above was also fit to the data with $\Gamma(Q)$ and τ_{ROT} as fitting parameters and b held constant at 1 Å. These fits invariably resulted in very large values of τ_{ROT} (i.e., the rotational contribution to the half-width becomes negligible) and $\Gamma(Q)$ converging to the same values as in the case of the one-Lorentzian case. Figure 5(a) shows the overall fit and the three components. The high quality of the fit is indicated by the values of χ^2 (typically below 3.5). The data from the sample heated to 373 K are also fitted in a similar manner and show no qualitative differences from the data measured at 300 K. Figure 5(b) presents the HWHM of the quasi-elastic component as a function of Q^2 for the two temperatures 300 K and 373 K. The increase of Γ with increasing Q reveals the existence of a fast translational jump diffusion process consistent with a distribution of jump lengths. Figure 5(b) also shows the best fit curve of the RJD model with the parameters in Table III.

Figure 6(a) shows an example of backscattering spectra measured on HFBS at 300 K. For the data analysis, we use seven spectra from detectors 6–12, corresponding to $Q^2 \sim 0.5$–2.0 Å^{-2}. The spectra measured at 300 K could not be accurately fitted using only one quasi-elastic component. Rather, they are well fitted by a combination of a narrow and a broad Lorentzian. The HWHM of the narrow Lorentzian component [Fig. 6(b)] corresponds to a slow translational diffusion process. The HWHM of the broad component [Fig.

TABLE III. Dynamical parameters for water in AMH-3 as extracted using the random jump diffusion model. Error estimates are given as uncertainties in the last reported decimal digit.

T (K)	Fast diffusion			Slow diffusion			Rotation
	D (m^2/s)	τ_0 (ps)	l (Å)	D (m^2/s)	τ_0 (ns)	l (Å)	τ_{ROT} (ps)
300	$2.0(5)\times10^{-9}$	9.0(7)	3.3(7)	$3.2(4)\times10^{-11}$	0.46(7)	3.0(5)	15.8(17)
373	$3.1(6)\times10^{-9}$	7.7(7)	3.8(9)	$7.3(8)\times10^{-11}$	0.35(9)	3.9(13)	
433				$8.4(5)\times10^{-11}$	0.13(3)	2.6 (3)	

6(c)] shows no systematic Q dependence, indicating that it originates from a rotational motion. However, the spectra collected at two higher temperatures (373 K and 433 K) are well fitted by a single Lorentzian which corresponds to the narrower component of the 300 K spectra and broadens as the temperature increases. The temperature dependence appears to follow a non-Arrhenius behavior [Fig. 6(b) and Table III]. The previously observed broad component no longer appears as a quasielastic contribution to the spectra, presumably because its HWHM (already comparable to the energy transfer window of HFBS at 300 K) broadens out further at higher temperatures so that it is no longer visible on HFBS. This rotational component is avoided in the DCS measurements by choosing an appropriate wavelength and Q range, as described earlier. In addition, the HWHM of this component is comparable to the resolution of the DCS instrument, so we do not expect to be able to observe it reliably at any momentum transfer on DCS. The average HWHM of the broad component at 300 K is calculated and used to extract the rotational relaxation time τ_{ROT}. The HWHMs of the narrow component are fitted by the RJD model to yield the corresponding diffusivities, residence times and root-mean-square jump distances (Table III). All the HFBS spectra are fit with $\chi^2<2.5$. The RJD model is one of several closely related jump diffusion models for characterizing water diffusion. Other models like the fixed jump diffusion model[29] or the Gaussian jump diffusion model[30] can also be used to interpret the data. However, in practice the different models give qualitatively similar results, especially within the moderately low Q values used in the present study.

Based on the data and fits of Figs. 5 and 6, it is clear that there are two different translational jump diffusion processes with similar length scales but widely separated in time scales, whose characteristics can be estimated by the RJD model parameters given in Table III. Previous QENS and molecular dynamics simulation studies[5–8] of water in layered oxides (containing a monolayer of water molecules in the interlayer spaces) agree that the translational motion of interlayer water is about an order-of-magnitude slower ($D\sim10^{-10}$ m^2/s) than in bulk water ($D\sim10^{-9}$ m^2/s at 295 K).[31] This is because the interlayer cations and the negatively charged terminal oxygen atoms of the oxide layers form strong bonds to the water molecules, resulting in hydration shells with a large water residence time and low diffusion coefficients compared to bulk water.[7,23] In the interlayer spaces of AMH-3, the above effects can be expected to be amplified because (a) there are 12 cations (including eight divalent strontium cations) for every 8 water molecules, and (b) there is a negatively charged terminal oxygen atom for

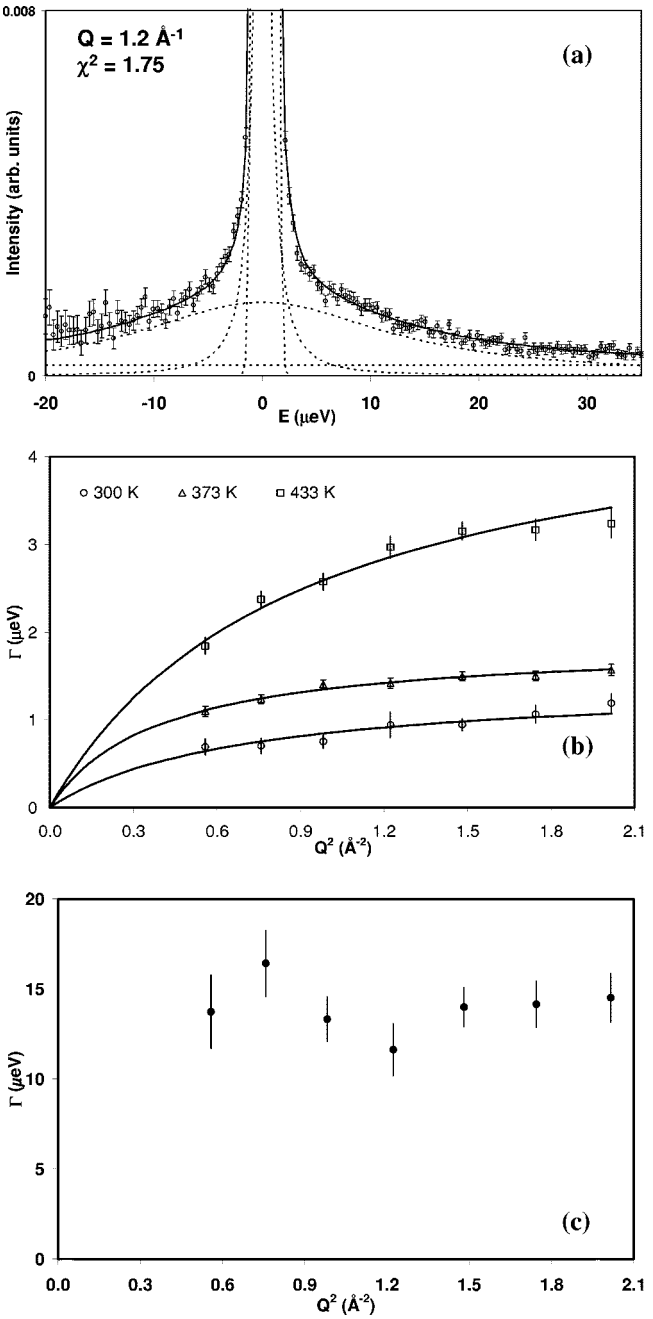

FIG. 6. (a) An example of the QENS spectrum from HFBS showing measured data and fitted components. (b) HWHM of the narrow quasielastic component observed on HFBS at three temperatures. The fits to the RJD model are shown as solid lines (after convolution with the instrumental resolution function). (c) HWHM of the broad component observed at 300 K.

every water molecule. As a result, water is likely to bind strongly to the cations (especially the divalent cations) and terminal oxygens. Hence, it seems logical to assign the observed slow diffusion and high residence time to the water molecules in the interlayer spaces of AMH-3. The jump distances (2.6–3.9 Å, Table III) extracted from the fits at different temperatures are also reasonable in comparison to the nearest neighbor *S*1-*S*1 crystallographic oxygen-to-oxygen distance (4.3 Å) in AMH-3. The situation in the porous layer spaces is rather different. There are only 4 monovalent sodium cations for every eight water molecules. Figure 1 shows that although the porous layers and interlayer spaces occupy about the same fractions of the unit cell volume, the porous layer is sparsely packed with cations and water molecules when compared to the interlayer spaces. This leads us to propose a high mobility for the water molecules in the porous layers, approaching that of bulk water at room temperature. The jump distance associated with this translational jump process is also consistent with the crystallographic nearest neighbor *S*2-*S*2 distance (3.8 Å), while the residence times are much lower than for water molecules in the interlayer spaces.

We also attempted to obtain molecular dynamics simulation data on water diffusion using two general-purpose interatomic force-field models,[32,33] to further examine our proposed interpretation of water transport mechanisms in AMH-3. However, the crystal structures and vibrational properties predicted by the two force fields are in poor agreement with experimental data, strongly indicating that more reliable force-field parametrizations are required for layered materials like AMH-3. Given the small size ($\sim 20\ \mu$m) of the platelike crystals obtained from the current synthesis procedure, only powder samples could be used in the present study. Since *S*1-*S*2 jumps would occur perpendicular to the layers and interlayers whereas *S*1-*S*1 and *S*2-*S*2 jumps occur parallel to the layers, these different types of jumps could be studied separately[7] if crystals of the material can be deposited with a high degree of out-of-plane orientation on a substrate. Similarly, a force field parametrized for structures like AMH-3 (with particular attention to the assignment of ionic charges) would allow simulations of water diffusion in AMH-3 to be performed, for a comparison with experimental results such as reported here.

VI. CONCLUSIONS

The three-dimensionally nanoporous crystalline layered silicate AMH-3 can be produced from a sodium-strontium-titanosilicate precursor solution within a certain window of compositions. ^{29}Si-NMR chemical shift anisotropy analysis and assignments of vibrational spectra confirm the previously determined x-ray structure of AMH-3. The transport properties of AMH-3 have been given detailed consideration. In particular, it has been shown experimentally by quasielastic neutron scattering, that water in AMH-3 exhibits two translational jump diffusion processes with widely different time scales but with similar length scales corresponding to jumps between water adsorption sites in the material. The diffusion properties extracted from our data, together with the details of the crystal structure, indicate that the two diffusion processes can be plausibly attributed to fast diffusion ($D \sim 10^{-10}$ m^2/s at 300 K) in the porous layers and slow diffusion ($D \sim 10^{-11}$ m^2/s) in the interlayer spaces.

ACKNOWLEDGMENTS

S.N. is grateful to the Georgia Institute of Technology, NIST, and the University of Maryland, for financial support. This work utilized facilities supported in part by the National Science Foundation (NSF) under Agreements No. DMR-0086210 (NIST) and CTS-0327811 (UMN). In addition, the development of the DAVE software package is supported by the NSF under Contract No. DMR-0086210.

*Corresponding author. Electronic address: sankar.nair@chbe.gatech.edu

[1] M. E. Davis, Nature (London) **417**, 813 (2002).
[2] H. Jobic, Curr. Opin. Solid State Mater. Sci. **6**, 415 (2002).
[3] R. Q. Snurr and J. Karger, J. Phys. Chem. B **101**, 6469 (1997).
[4] J. Kärger, S. Vasenkov, and S. M. Auerbach, in *Handbook of Zeolite Science and Technology*, edited by K. A. Carrado, P. K. Dutta, and S. M. Auerbach (Marcel Dekker, New York, 2003), p. 341.
[5] S. Takahara, S. Kittaka, Y. Kuroda, T. Yamaguchi, H. Fujii, and M. C. Bellissent-Funel, Langmuir **16**, 10 559 (2000).
[6] J. Swenson, R. Bergman, D. T. Bowron, and S. Longeville, Philos. Mag. B **82**, 497 (2002).
[7] J. Swenson, R. Bergman, and W. S. Howells, J. Chem. Phys. **113**, 2873 (2000).
[8] V. Marry, P. Turq, T. Cartailler, and D. Levesque, J. Chem. Phys. **117**, 3454 (2002).
[9] H. K. Jeong, S. Nair, T. Vogt, L. C. Dickinson, and M. Tsapatsis, Nat. Mater. **2**, 53 (2003).
[10] B. Wei, J. H. Yu, Z. Shi, S. L. Qiu, and J. Y. Li, J. Chem. Soc. Dalton Trans. **13**, 1979 (2000).
[11] L. Vidal, C. Marichal, V. Gramlich, J. Patarin, and Z. Gabelica, Chem. Mater. **11**, 2728 (1999).
[12] A. Corma, V. Fornes, S. B. Pergher, T. L. M. Maesen, and J. G. Buglass, Nature (London) **396**, 353 (1998).
[13] E. L. Cussler, S. E. Hughes, W. J. Ward, and R. Aris, J. Membr. Sci. **38**, 161 (1988).
[14] J. R. D. Copley and J. C. Cook, Chem. Phys. **292**, 477 (2003).
[15] A. Meyer, R. M. Dimeo, P. M. Gehring, and D. A. Neumann, Rev. Sci. Instrum. **74**, 2762 (2003).
[16] Data Analysis & Visualization Environment (DAVE), www.ncnr.nist.gov/dave.
[17] A. J. Iggo, *NMR Spectroscopy in Inorganic Chemistry* (Oxford University Press, Oxford, 1999).
[18] E. M. Flanigen, H. Khatami, and H. A. Seymenski, in *Advances in Chemistry Series*, edited by E. M. Flanigen and L. B. Sand

(American Chemical Society, Washington D.C., 1971), Vol. 101, p. 201.

[19] E. Geidel, H. Sohlig, C. Peuker, and W. Pilz, in *Studies on Surface Science and Catalysis*, edited by G. Ohlmann, H. Pfeifer, and R. Fricke (Elsevier, Amsterdam, 1991), Vol. 65, p. 511.

[20] K. Nakamoto, *Infrared and Raman Spectra of Inorganic and Coordination Compounds* (Wiley, New York, 1986).

[21] J. Teixeira, M. C. Bellissent-Funel, and S. H. Chen, J. Phys.: Condens. Matter **2**, SA105 (1990).

[22] M. C. Bellissent-Funel, S. H. Chen, and J. M. Zanotti, Phys. Rev. E **51**, 4558 (1995).

[23] H. Paoli, A. Methivier, H. Jobic, C. Krause, H. Pfeifer, F. Stallmach, and J. Karger, Microporous Mesoporous Mater. **55**, 147 (2002).

[24] O. Borodin, F. Trouw, D. Bedrov, and G. D. Smith, J. Phys. Chem. B **106**, 5184 (2002).

[25] D. J. Cebula, R. K. Thomas, and J. W. White, Clays Clay Miner. **29**, 241 (1981).

[26] M. C. Bellissent-Funel, J. M. Zanotti, and S. H. Chen, Faraday Discuss. **103**, 281 (1996).

[27] W. F. Sears, Can. J. Phys. **44**, 1299 (1966).

[28] L. Liu, A. Faraone, and S. H. Chen, Phys. Rev. E **65**, 041506 (2002).

[29] A. Renouprez, P. Fouilloux, R. Stockmeyer, H. M. Conrad, and G. Goeltz, Ber. Bunsenges. Phys. Chem. **81**, 429 (1977).

[30] J. J. Tuck, P. L. Hall, M. H. B. Hayes, D. K. Ross, and J. B. Hayter, J. Chem. Soc., Faraday Trans. **81**, 833 (1985).

[31] J. Teixeira, M. C. Bellissent-Funel, and S. H. Chen, J. Mol. Liq. **48**, 123 (1991).

[32] A. K. Rappe, C. J. Casewit, K. S. Colwell, W. A. Goddard, and W. M. Skiff, J. Am. Chem. Soc. **114**, 10024 (1992).

[33] H. Sun, J. Phys. Chem. B **102**, 7338 (1998).